Catalysis Today 413–415 (2023) 113996

Contents lists available at ScienceDirect

Catalysis Today

journal homepage: www.elsevier.com/locate/cattod

Innovative photoelectrocatalytic water remediation system for ammonia abatement

Simone Livolsi [a], Silvia Franz [b], Annamaria Costa [c], Eleonora Buoio [c], Chiara Bazzocchi [c], Massimiliano Bestetti [b], Elena Selli [a], Gian Luca Chiarello [a,*]

[a] Department of Chemistry, Università degli Studi di Milano, Via Golgi 19, 20133 Milano, Italy
[b] Department of Chemistry, Materials and Chemical Engineering "Giulio Natta", Politecnico di Milano, Piazza Leonardo da Vinci 32, 20133 Milano, Italy
[c] Department of Veterinary Medicine and Animal Science, Università degli Studi di Milano, Via dell'Università 6, 26900 Lodi, Italy

ARTICLE INFO

Keywords:
Photoelectrocatalysis
Ammonia abatement
Water remediation
PEO

ABSTRACT

Ammonia, produced by human and animal activities, contributes to water and soil pollution because it is toxic for aquatic flora and fauna, and responsible for eutrophication. In this work, the photoelectrocatalytic (PEC) oxidation of ammonia is investigated employing a stainless-steel PEC reactor, consisting of a central UV Hg-vapor lamp surrounded by a metallic Ti mesh coated with a photoactive TiO_2 film, directly grown by Plasma Electrolytic Oxidation (PEO). The so prepared TiO_2 film is characterized by XRD, SEM, UV–vis DRS and IPCE. The PEC reactor operates at 4 V potential drop between the TiO_2 coated mesh (photoanode) and the body of the reactor (cathode). The effect of the operating parameters (recirculation flowrate and air bubbling) and type of electrolyte solution (KCl or K_2SO_4) on the PEC performance are investigated in terms of ammonia conversion and selectivity to nitrite, nitrate and molecular nitrogen. Full ammonia conversion (X_{NH3}) with a selectivity to molecular nitrogen up to 67 % are attained after 12 h in 5 mM KCl electrolyte solution. Nitrite is produced within the first 6 h irradiation and then fully converted into nitrate. By contrast, only a slight X_{NH3} (ca. 10 %) is observed in K_2SO_4 electrolyte solution. These results suggest that chlorine has a crucial role in the ammonia PEC oxidation process: photo-generated holes on the photoanode surface can oxidize Cl^- to $Cl^\bullet$ (electro-induced process), which is a reactive radical able to oxidase ammonia.

1. Introduction

Nitrogen-containing compounds produced by human activities have greatly perturbed the global nitrogen cycle in the last century. Because the perturbation of the nitrogen cycle is considered as one of the planetary boundaries already trespassed, we urgently need to develop new, more efficient and environmentally friendly water treatment technologies for N-content remediation. Animals, including fishes, convert the nitrogen content of food and nutrients into ammonia (NH_3), which is successively oxidized mainly into nitrite (NO_2^-) and nitrate (NO_3^-) anions by means of different chemical and biological processes [1]. High levels of nitrogen compounds in aquatic ecosystems can compromise the capability of animals to grow, reproduce and survive [2]. Indeed, ammonia can provoke asphyxiation, inhibition of ATP production and repression of immune system, while its protonated form (NH_4^+) seems to be less toxic. Nitrites are even more toxic than ammonia itself, forming mutagenic and carcinogenic N-nitroso compounds, which damage mitochondria in liver cell tissues and decrease tolerance to parasitic and bacterial diseases. Finally, the toxicity of nitrate in aquatic ecosystems is traditionally considered to be irrelevant [3]. Moreover, acidification of freshwater, eutrophication and the occurrence of toxic algae are the most impacting consequences of the accumulation of ammonia and its derivatives in the ecosystems.

Different remediation methods can be adopted to remove ammonia from aquatic ecosystems [4]. The most diffuse method is bioremediation via nitrification-denitrification, the first aerobic step of which consists in ammonia oxidation to nitrates that are subsequently converted into gaseous nitrogen by heterotrophic microorganisms in the second anaerobic step. The main advantages of biological remediation technologies are the high selectivity and the biocompatibility, but any variation in pH, temperature or feed composition can dramatically affect the activity of microorganisms and thus the efficiency of pollutants removal [5,6]. The physico-chemical remediation methods include ammonia stripping, chemical or electrochemical oxidation or separation

* Corresponding author.
E-mail address: gianluca.chiarello@unimi.it (G.L. Chiarello).

https://doi.org/10.1016/j.cattod.2023.01.003
Received 30 August 2022; Received in revised form 21 December 2022; Accepted 2 January 2023
Available online 3 January 2023

by means of selective membranes. Despite biological technologies are the most largely employed, they are less efficient and require longer time compared to the other treatments [7,8].

Photocatalysis belongs to the family of innovative advance oxidation technologies that can be exploited for ammonia oxidation [9–15]. In particular, a TiO_2-based photocatalytic system has been successfully employed for water treatment and ammonia remediation in zebrafish [16] and rainbow trout [17] aquaculture and in livestock manure [18]. Moreover, the advantage of photocatalysis applied to real systems is its additional antibacterial and antiviral effect [19,20].

In this work, we explore the possibility of boosting the photocatalytic performance in ammonia abatement by applying an external electrical bias. For this purpose, we have investigated an innovative photoelectrochemical (PEC) reactor that combines a commercial water-UV sterilizer with a photoactive TiO_2-coating directly grown on a metallic Ti mesh by plasma electrolytic oxidation (PEO), acting as photoanode [21].

Because both fresh- or sea-water contain a significant amount of dissolved chloride, the PEC system can further exploit the UV/electrochlorine advanced oxidation process [22,23], occurring in chloride based electrolytic solutions, where the Cl^- anion is oxidized by photogenerated holes to chlorine radical (E° $Cl^\bullet/Cl^- = 2.47$ V vs. NHE), which is highly reactive and selective in ammonia oxidation yielding molecular nitrogen or nitrate.

2. Material and methods

2.1. TiO_2 photoanodes preparation via plasma electrolytic oxidation

The photoactive TiO_2 coated mesh preparation and the description of the photoreactor design is extensively reported elsewhere [24]. Here briefly, the TiO_2 film for this PEC application was directly grown over a metallic Ti mesh (photoanode) via Plasma Electrolytic Oxidation (PEO), a plasma-assisted technology for single step preparation of large area TiO_2 photoanodes, allowing the fast conversion of a metallic surface into a crystalline metal oxide film.

The TiO_2 coated Ti mesh was prepared at 150 V in H_2SO_4 1.5 mol L^{-1} at − 5 °C for 5 min, following the previously reported experimental procedure [25].

2.2. TiO_2 photoanodes characterization

The morphology and pore diameter of the TiO_2 coating were investigated by Scanning Electron Microscopy (SEM, Zeiss EVO50). The crystal phase composition was studied by X-ray diffraction (XRD, Philips PW1830), by using Cu Kα radiation (λ = 1.5418 Å). The band-gap energy was measured from the Tauc-plot. The UV–vis–NIR diffuse reflectance (UV–vis DRS) spectra were recorded in the 220–2600 nm wavelength range with a Shimadzu UV3600 Plus spectrophotometer equipped with an ISR-603 integrating sphere.

The incident photon-to-current efficiency (IPCE) curve was measured at 1.0 V vs. SCE in a Na_2SO_4 0.5 mol L^{-1} electrolyte solution, on an optical bench already described elsewhere [26]. IPCE is calculated by measuring, at a fixed wavelength (λ), the power of the incident radiation (P_{in}) and the generated photocurrent (I):

$$IPCE = \frac{1240 \times I(Acm^{-2})}{\lambda(nm) \times P_{in}(Wcm^{-2})}$$

2.3. Photocatalytic tests

A schematic representation of the setup employed for the PEC tests is reported in Fig. 1. It consists of a stainless-steel reactor with cylindrical shape (diameter 6 cm, length 22 cm and free volume 430 mL), with a commercial 30 W medium-pressure Hg-vapor lamp arranged at the central axis of the reactor, surrounded by the TiO_2-coated titanium mesh. A rotary pump inside an external 3 L tank provides a recirculation flowrate from 120 to 350 L h^{-1}. The PEC reactor works at constant potential drop applied between the TiO_2 coated mesh (photoanode) and the body of the reactor (cathode) by means of an Amel Model 2549 potentiostat.

Two types of PEC tests have been performed using this experimental setup: *i*) The effects of the electrolyte (KCl 5 mM, KCl 500 mM or K_2SO_4 2.5 mM) and operating parameters (air bubbling, recirculating flow rate of 120 or 350 L h^{-1} and applied cell voltage of 2 or 4 V) were investigated by recirculating 3 L of electrolyte solution with an ammonia concentration of 20 ppm or 100 ppm; *ii*) Tests under ammonia dropping conditions were performed by recirculating an initial volume of electrolyte solution equal to 1.5 L, then other 1.5 L of the same electrolyte solution but containing 4 or 40 ppm ammonia were added dropwise in 8 h using a syringe pump. This latter experiment simulates a sort of

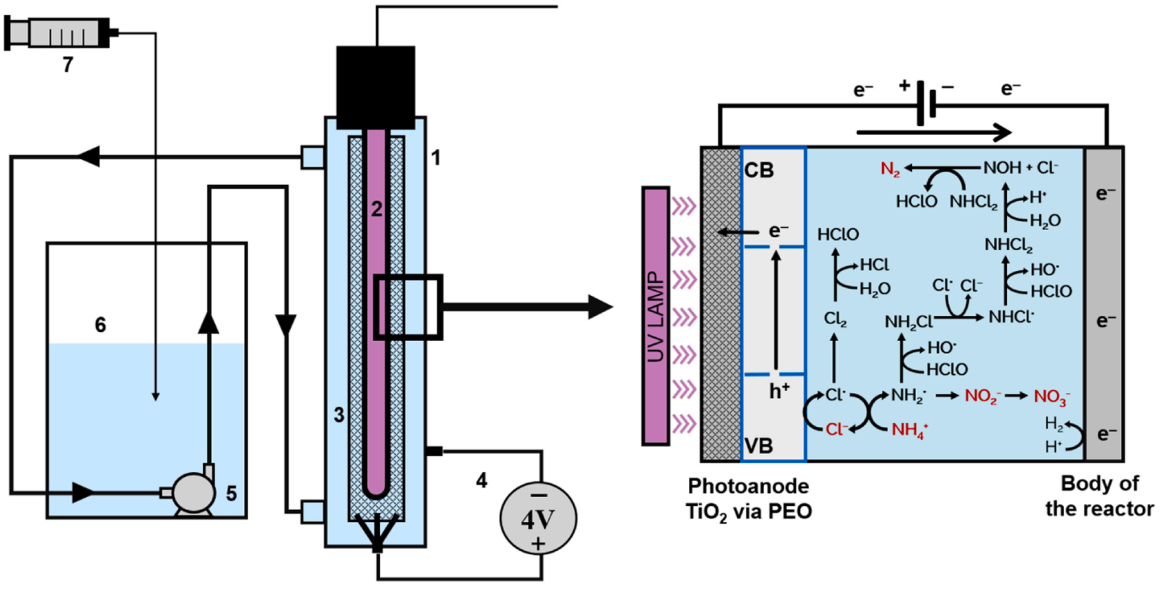

Fig. 1. Schematic of the PEC reactor and experimental setup: (1) PEC reactor, (2) UV-lamp, (3) TiO_2 coated mesh, (4) potentiometer, (5) rotary pump, (6) external tank and (7) syringe pump. The PEC oxidation scheme of indirect ammonia oxidation involving chlorine ions is reported on the right.

constant ammonia release such as that due to excretion by fishes in a tank. Finally, linear sweep voltammetry (LSV) analysis was performed by applying a cell voltage from 0 to 6 V with an increment of 10 mV s^{-1} in a KCl 5 mM electrolyte solution.

2.4. Analytical methods and calculations

The concentration of ionic species in water was monitored by means of an ion chromatograph (Metrohm, 761 Compact IC with conductivity detector) after sampling the recirculating water every hour. A typical cation and anion chromatogram is shown in Fig.S1.

In recirculating tests, the conversion of ammonia (X_{NH3}) and the selectivity to each product (S_i, with i = NO_2^-, NO_3^- and N_2) were calculated from the initial NH_4^+ concentration in the recirculated solution ($C_{NH4^+,i}$) and the concentration of NH_4^+, NO_2^- and NO_3^- in each sample ($C_{NH4^+,t}$, $C_{NO2^-,t}$ and $C_{NO2^-,t}$), as follows:

$$X_{NH_3} = \frac{C_{NH_4^+,i} - C_{NH_4^+,t}}{C_{NH_4^+,i}} \times 100 \quad (1)$$

$$S_{NO_2^-}\% = \frac{C_{NO_2^-,t}}{C_{NH_4^+,i} - C_{NH_4^+,t}} \times 100 \quad (2)$$

$$S_{NO_3^-}\% = \frac{C_{NO_3^-,t}}{C_{NH_4^+,i} - C_{NH_4^+,t}} \times 100 \quad (3)$$

$$S_{N_2}\% = 100 - S_{NO_2^-}\% - S_{NO_3^-}\% \quad (4)$$

All concentration, conversion and selectivity values are reported as a function of the irradiation time (t_i) and of the operating time (t_o), which represents the normalized irradiation time, considering the ratio between the free volume of the reactor (V_r), the volume of treated water (V_t) and, eventually, the dropping flowrate (F_{drop}) and initial volume (V_i):

For recirculating tests: $t_o = t_i \frac{V_r}{V_t}$.

For tests under dropping conditions: $t_o = t_i \frac{V_r}{V_i + (F_{drop} \times t_i)}$.

This is necessary because the volume of treated water is higher than the inner free volume of the reactor, so the residence time inside the reactor does not coincide with the irradiation time.

3. Results and discussion

3.1. TiO_2 photoanode characterization

The SEM micrograph reported in Fig. 2A shows the characteristic sponge-like morphology and the complex interconnected structure of PEO-grown coatings, with an average pore size diameter equal to 472 ± 132 nm. X-ray diffraction (XRD) was employed to evaluate the crystalline structure and composition of the TiO_2 film, resulting in a phase composition of 45 % rutile and 55 % anatase (Fig. 2B). The Tauc plot of the UV–vis DRS analysis (Fig. 2D) gives a band gap energy of ca. 3.08 eV, typical of the rutile phase, corresponding to a ca. 403 nm wavelength. This value was confirmed by IPCE analysis (Fig. 2C) that shows a photoactivity threshold located below 410 nm. Two relative IPCE maxima are present at 374 nm (IPCE 50 %) and 315 nm (IPCE 72 %), that could be attributed to the superposition of the rutile and anatase phase photoactivity, respectively. Indeed, the anatase phase possesses a wider band gap energy of 3.2 eV, corresponding to a wavelength of ca. 387 nm, with respect to that of rutile (3.0 eV and 413 nm).

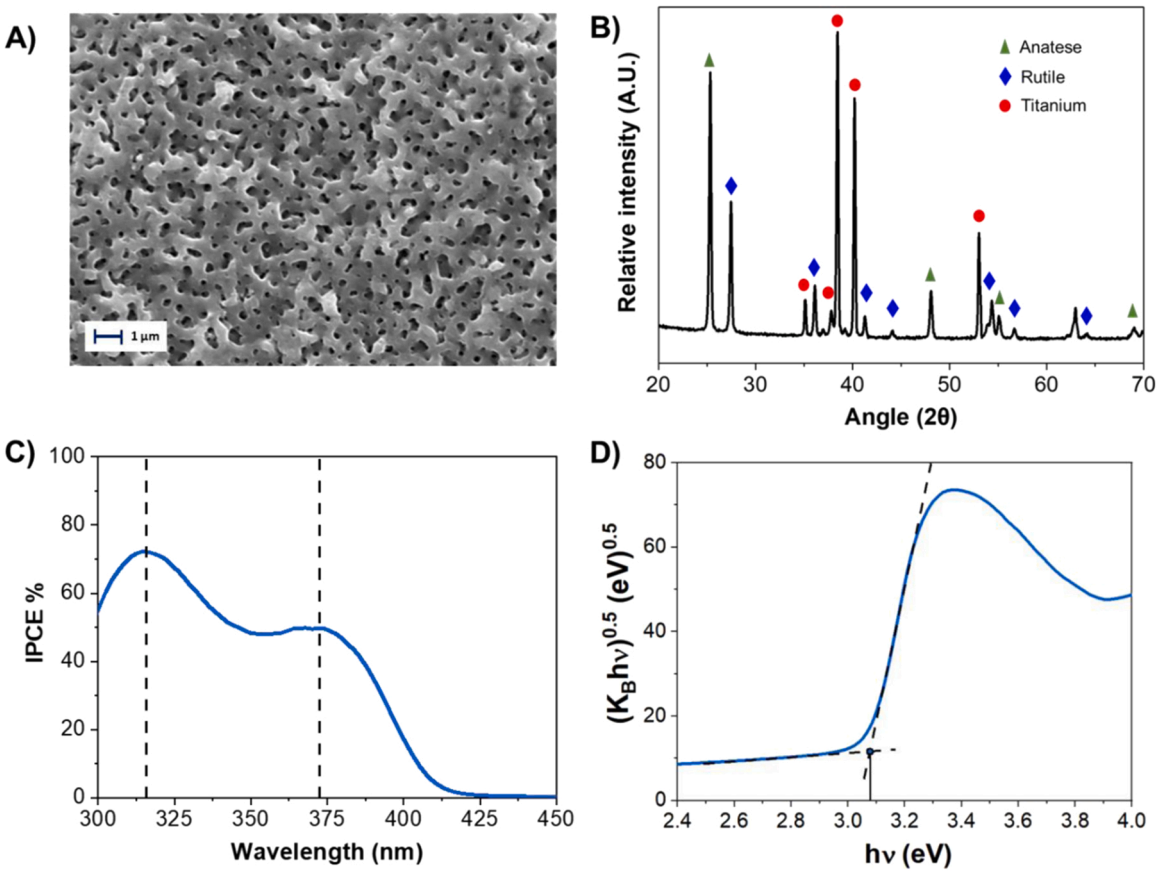

Fig. 2. Characterization of the as prepared TiO_2 coating grown by PEO on a metal Ti mesh: (A) SEM image, (B) XRD pattern, (C) IPCE analysis measured at 1.0 V vs. SCE in Na_2SO_4 0.5 M electrolyte solution and (D) Tauc plot from UV-Vis DRS.

3.2. Effect of operating conditions on the PEC performance under recirculating conditions

Typical NH_3, NO_2^- and NO_3^- concentration profiles during irradiation at 4 V in KCl 5.0 mM and 120 L h^{-1} recirculation flowrate are shown in Fig. 3. Ammonia concentration decreases almost linearly reaching a ca. 75 % conversion after 8 h irradiation time (1.14 h operating time). Meanwhile, nitrite concentration reaches a maximum of ca. 3 ppm after 2 h, then its concentration decreases below the detection limit after 7 h, while nitrate concentration follows a sigmoid-like profile. This trend is characteristic of the kinetics of consecutive reactions, with nitrite as intermediate in ammonia oxidation up to nitrate (Eqs. (5) and (6)).

However, nitrite and nitrate formation only accounts for ca. 50 % of the converted ammonia (Fig. 4). Hence, the rest of ammonia is oxidized to gaseous molecular nitrogen, although we cannot exclude the formation of NOx species. Because hydrogen evolution ($2H^+ + 2e^- \rightarrow H_2$) simultaneously occurs at the cathode, N_2 is then produced via an inverse ammonia synthesis reaction (Eq. (7)). Hence, the PEC oxidation of aqueous ammonia follows two parallel pathways [27]:

$$NH_3 + \frac{3}{2}O_2 \xrightarrow{TiO_2+h\nu} NO_2^- + H_2O + H^+ \quad (5)$$

$$NO_2^- + \frac{1}{2}O_2 \xrightarrow{TiO_2+h\nu} NO_3^- \quad (6)$$

$$2NH_3 \xrightarrow{TiO_2+h\nu} N_2 + 3H_2 \quad (7)$$

The first oxidation path is the conversion of ammonia into nitrate through a consecutive reaction mechanism with nitrite as intermediate species (Eqs. 5 and 6), while in the second case ammonia is oxidized into gaseous nitrogen (Eq. (7)), i.e., into an inert and non-toxic gaseous compound. Since nitrite is even more toxic than ammonia, the second path is the favorite one leading to harmless molecular nitrogen.

The effect of initial ammonia concentration (C°_{NH3} = 100 or 20 ppm), air bubbling, recirculating flow rate (120 or 350 L h^{-1}) and applied voltage (2 or 4 V) on ammonia conversion and selectivity to nitrite, nitrate and nitrogen are reported in Fig. 4.

Air bubbling (10 L h^{-1} fed at the reactor inlet) is expected to increase the amount of dissolved oxygen and the turbulence inside the reactor, demonstrates to have a detrimental effect on both ammonia conversion (decreasing from 15 % to only 8 % after 6 h) and selectivity to nitrate (Fig. 4A) under these PEC reaction conditions.

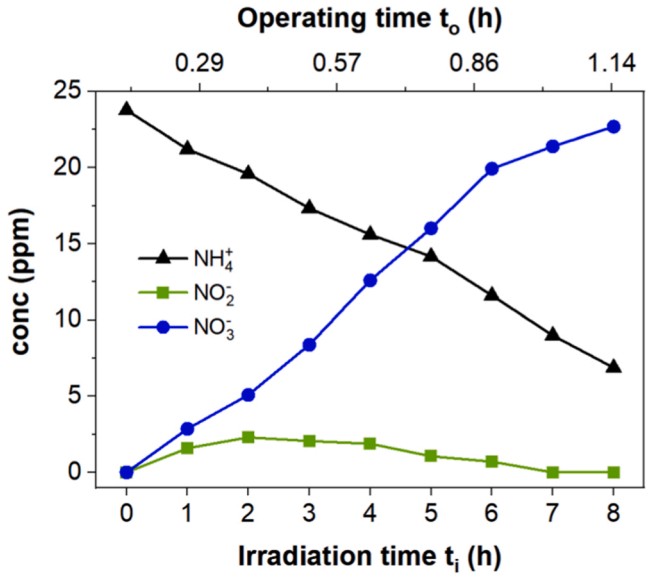

Fig. 3. NH_4^+, NO_2^- and NO_3^- concentration profiles at 4 V in a KCl 5.0 mM electrolyte solution with 120 L h^{-1} recirculating flowrate.

On the other hand, by decreasing C°_{NH3} from 100 (Fig. 4A) to 20 ppm (Fig. 4B) there is a fourfold increase of X_{NH3}, from 15 up to 60% after 6 h irradiation. Furthermore, Fig. 5 shows that the ammonia conversion rate, given by the slope of the straight line interpolating the NH_3 concentration vs. operation time, is independent of the initial ammonia concentration (r_{NH3} = 0.80 vs. 0.85 $mmol_{NH3}$ L^{-1} h^{-1}, with C°_{NH3} of 20 or 100 ppm, respectively). This confirms the pseudo zero order rate of ammonia conversion under the here adopted PEC conditions.

The recirculation flowrate is a more important operating parameter affecting the residence time of the species inside the reactor. As expected, a higher X_{NH3} is attained at lower flowrate (Fig. 4B), increasing from 56 % at 350 L h^{-1} to 71 % at 120 L h^{-1} after an 8 h. Interesting, S_{N2} also increased by decreasing the flow rate, passing from 44 % at 350 L h^{-1} to 67 % at 120 L h^{-1}. Hence, longer residence time seems to promote the reaction mechanism of ammonia oxidation to molecular nitrogen rather than those yielding to nitrite and nitrate. A total ammonia conversion was reached after 12 h irradiation with a final S_{N2} up to 67 %, working at 120 L h^{-1} flowrate. Finally, the effect of the applied cell voltage are shown in Fig. 4C and Fig. S2. At 2 V, steady state conditions were reached only after 2 h irradiation, attaining a lower value than when operating at 4 V (after 8 h X_{NH3} was 70 % at 4 V and 55 % at 2 V). Indeed, the applied cell voltage can affect the charge separation and, consequently, the generated photocurrent and ammonia conversion. By decreasing the cell voltage from 4 V to 2 V, the average photocurrent measured during the test decreased from 154 to 84 mA (Fig. S2A), while the ammonia conversion rate r_{NH3} decreased from 0.84 to 0.47 mmol L^{-1} h^{-1} (Fig. S2B). Interestingly, the ratio of averaged photocurrent generated at 4 V and 2 V (184/84 = 1.80) is similar to the corresponding ratio of r_{NH3} (0.84/0.47 = 1.79). This result demonstrates that r_{NH3} is directly proportional to the photocurrent. Moreover, the chronoamperometry test (Fig. S2A) shows a good time on stream stability of the generated photocurrent during the 8 h-long ammonia degradation photocatalytic test.

3.3. Effect of electrolyte nature and concentration

Two different electrolytes have been investigated: KCl 5 mM and K_2SO_4 2.5 mM (Fig. 5). Interestingly, no ammonia conversion was observed in K_2SO_4 despite the similar photocurrent (ca. 150 mA) recorded with the two electrolytes. This result highlights the crucial rule of chloride in the PEC oxidation of ammonia. To further explore the effect of chloride we investigated the effect of KCl concentration of 5 mM and 500 mM, simulating the salinity of freshwater and salty water. Increasing chloride concentration led to ca. fivefold increase in ammonia reaction rate from 0.85 up to 3.86 $mmol_{NH3}$ L^{-1} h^{-1}, while the photocurrent increased only from 150 to 175 mA. The PEC system can exploit the UV/electro-chlorine advanced oxidation process [22,28,29]. In this process, the photo-generated holes on the TiO_2 surface can oxidize, in the presence of an electrical bias, chloride ions into $Cl^\bullet$ radical (E° $Cl^\bullet/Cl^-$ = 2.47 V vs. NHE) (Eq. (10)). This electro-chlorine process inhibits the oxidation of water into $OH^\bullet$ (Eq. 9), that is the typical reactive species, together with O_2^-, involved in tradition photocatalytic oxidation processes. Chlorine radicals can follow different reaction pathways, including the formation of molecular chlorine (Cl_2) (Eq. (11)), which further evolves into hypochlorous acid (HClO) (Eq. (12)). These highly reactive species can react with ammonia, leading to its conversion into N_2 or other oxidation products (Fig. 1). In particular, the reaction of ammonium cation with chlorine radical produces amino radical $NH_2^\bullet$ (Eq. (13)), which can further react following two different paths leading to the final formation of molecular nitrogen or nitrite and nitrate:

Path 1) Reaction of amino radical with hypochlorous acid or chlorine radical forming different chloramines intermediates, including monochloramine (NH_2Cl) and dichloramine ($NHCl_2$) according to Eqs. (14)–(16). Dichloramine can decompose to molecular nitrogen reacting either with monochloramine (Eq. (17)) or with water through the formation of

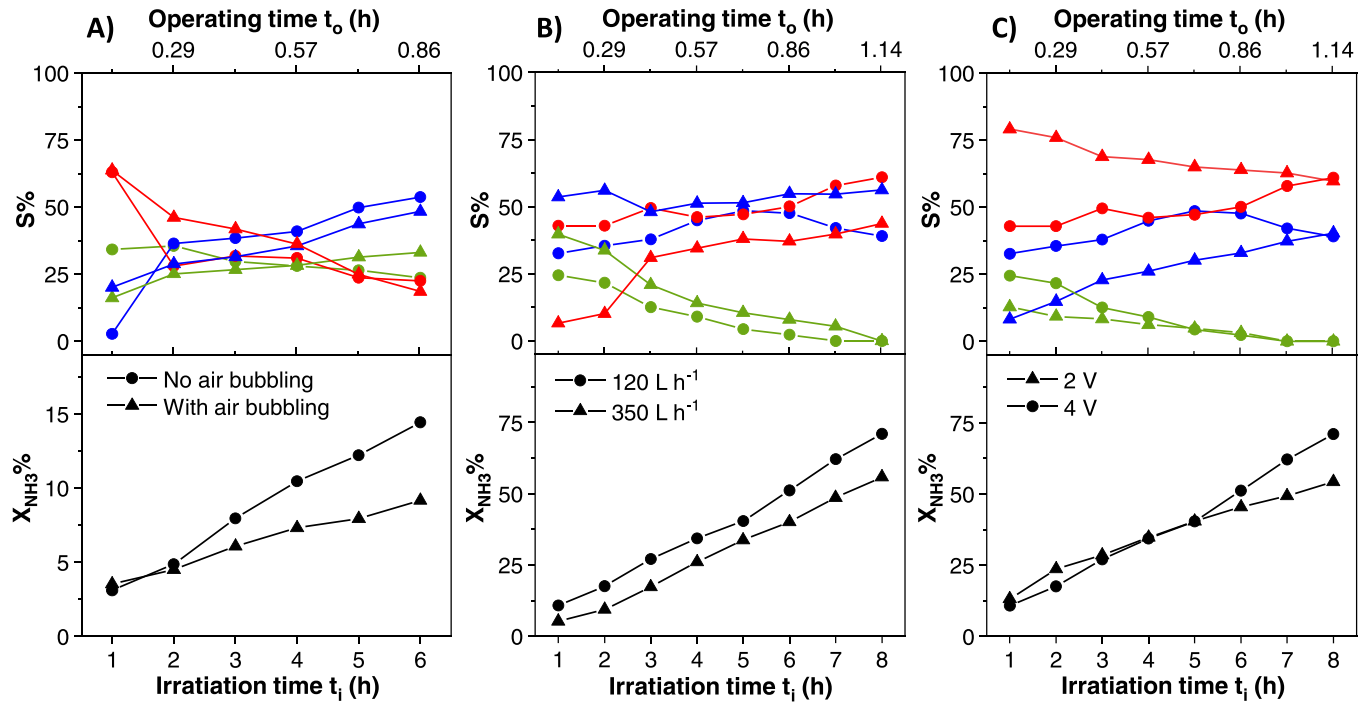

Fig. 4. Effect of operating parameters on ammonia conversion (black lines) and selectivity to nitrite (green lines), nitrate (blue lines) and molecular nitrogen (red lines): A) air bubbling (C°_{NH3} = 100 ppm, 4 V and 120 L h^{-1}), B) recirculation flowrate (C°_{NH3} = 20 ppm and 4 V), and C) applied cell voltage (C°_{NH3} = 20 ppm and 120 L h^{-1}). All tests performed in KCl 5 mM electrolyte solutions.

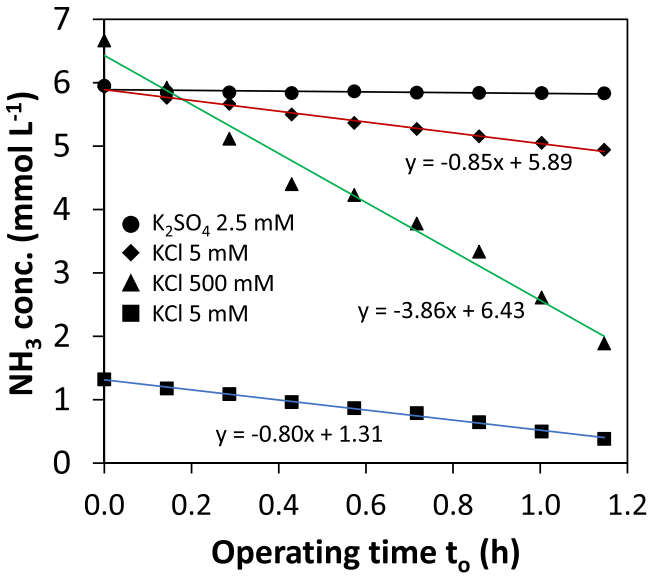

Fig. 5. Effect of electrolyte nature (K_2SO_4 circles or KCl diamonds), initial ammonia concentration (100 ppm diamonds or 20 ppm squares) and KCl concentration (5 mM diamonds or 500 mM triangles) on the ammonia concentration variation during PEC oxidation at 4 V and 120 L h^{-1} recirculation flow rate.

nitroxyl (HNO) as intermediate (Eqs. (18) and (19)). Indeed, nitroxyl is a short-lived intermediate and rapidly decomposes to nitrous oxide (N_2O) or reacts with $NHCl_2$ to form N_2 (Eq. (19)).

Path 2) Reaction of amino radical with hydroxyl radical yielding hydroxylamine (Eq. (20)) which can further oxidize into nitrite and nitrate (Eq. (21)).

$$TiO_2 + h\nu \rightarrow h^+ + e^- \quad (8)$$

$$H_2O + h^+ \rightarrow HO^\bullet + H^+ \quad (9)$$

$$Cl^- + h^+ \rightarrow Cl^\bullet \quad (10)$$

$$2Cl^\bullet \rightarrow Cl_2 \quad (11)$$

$$Cl_2 + H_2O \rightarrow HClO + HCl \quad (12)$$

$$NH_4^+ + Cl^\bullet \rightarrow NH_2^\bullet + Cl^- + 2H^+ \quad (13)$$

$$HClO + NH_2^\bullet \rightarrow NH_2Cl + HO^\bullet \quad (14)$$

$$NH_2Cl + Cl^\bullet \rightarrow NHCl^\bullet + Cl^- + H^+ \quad (15)$$

$$NHCl^\bullet + HClO \rightarrow NHCl_2 + HO^\bullet \quad (16)$$

$$NHCl_2 + NH_2Cl \rightarrow N_{2(g)} + 3H^+ + 3Cl^- \quad (17)$$

$$NHCl_2 + H_2O \rightarrow HNO + 2H^+ + 2Cl^- \quad (18)$$

$$NHCl_2 + HNO \rightarrow N_{2(g)} + HClO + H^+ + Cl^- \quad (19)$$

$$NH_2^\bullet + HO^\bullet \rightarrow NH_2OH \quad (20)$$

$$NH_2OH + HO^\bullet \rightarrow NO_2^- \rightarrow NO_3^- \quad (21)$$

Although this reactions sequence is only speculative, as no intermediate species has been detected in this work, the elementary reactions involved in the UV/chlorine assisted decomposition of ammonia, including the reactivity of intermediate chloramine, are widely reported in literature and are recently summarized by Kwon et al. [30], who also reported the reaction rate constants.

Thus, working with both UV light and potential bias, chloride ion is the main reactive specie responsible for ammonia oxidation. This explains why no significant ammonia conversion is observed in the absence of a chloride-based electrolyte or when increasing the dissolved oxygen content in water by air bubbling.

3.4. PEC test under dropping conditions

In order to simulate a continuous production of ammonia, as in fish farming tanks, a test was performed under dropwise addition, to an initial volume of 1.5 L of KCl 5 mM, of an identical volume of the same electrolyte solution containing 4 or 40 ppm of ammonia in 8 h using a syringe pump (i.e., with a flowrate of 187.5 mL h^{-1}). This test allows to evaluate the ability of this PEC system in avoiding ammonia accumulation in close recirculating aquatic systems.

Neither NH_4^+ nor NO_2^- were ever detected over time upon dropping the 4 ppm ammonia solution. Only NO_3^- was linearly accumulated in water up to 4.7 ppm after 8 h (t_o 1.15 h). This means that all added ammonia was immediately converted into N_2 or NO_3^-, with selectivity of 45 % and 55 %, respectively, and without accumulation of toxic nitrite.

By increasing to 40 ppm the concentration of the dropped ammonia solution, NH_4^+ concentration first increases up to a maximum value of 5.7 ppm after 4 h (t_o 0.8 h), then it reaches a plateau with X_{NH3} up to 75 %. Also in this case, no nitrite was detected, i.e., no oxidation intermediates were accumulated over time. Nitrate concentration increased linearly, reaching a concentration of 12.5 ppm after 8 h. In these conditions S_{N2} remained in the 73–80 % range along the whole test.

3.5. Stability of the PEC reactor

Linear sweep voltammetry (LSV) analyses were periodically performed to evaluate the stability of the PEC reactor over time before and after every PEC test. The LSV curves after 0, 12, 24, 36, 52, 68 and 160 irradiation hours are shown in Fig. 6. A slight irreversible decrease of photocurrent at 1 V was observed over time, whereas at 4 V the photocurrent decreased from 135 mA down to a minimum of 108 mA after 52 h and then raised up again to 138 mA after 162 h irradiation time. Thus, no significant changes in PEC performance were detected over time, highlighting the robustness and the stability of the TiO_2 coated mesh produced by PEO.

4. Conclusion

The here tested photoelectrocatalytic reactor could be successfully employed in water remediation systems for the abatement of the total ammonia nitrogen (TAN) in recirculating aquaculture systems (RAS). Ammonia concentration above 1.5 ppm is considered toxic for most fish, while the acceptable level in RAS is usually set at 0.025 ppm. Tests performed under dropping conditions have shown that this ammonia level could be attained with a proper scale-up. Furthermore, the advantage of the PEC system compared to a traditional biological nitrification unit is the possibility of lowering the total nitrogen content of the recirculating water thanks to a high selectivity to gaseous nitrogen. Finally, this work demonstrates that the PEC system exploits the UV/electro-chlorine process to oxidize ammonia. Chloride is present in all real water ecosystem and it turns particularly effective in seawater.

CRediT authorship contribution statement

Simone Livolsi: Validation, Investigation, Writing – original draft. **Silvia Franz:** Methodology, Resources, Writing – review & editing. **Annamaria Costa:** Methodology, Resources, Funding acquisition. **Eleonora Buoio:** Investigation. **Chiara Bazzocchi:** Methodology, Resources, Funding acquisition. **Massimiliano Bestetti:** Methodology, Resources. **Elena Selli:** Conceptualization, Methodology, Resources, Writing – review & editing, Supervision, Project administration, Funding acquisition. **Gian Luca Chiarello:** Conceptualization, Methodology, Validation, Resources, Writing – review & editing, Supervision, Project administration, Funding acquisition.

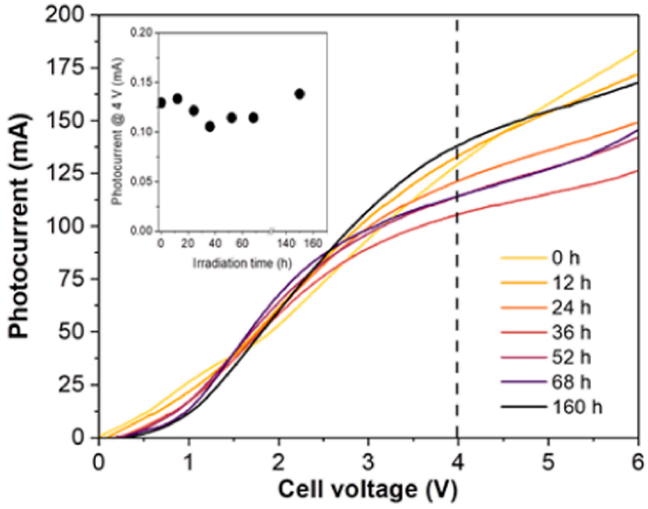

Fig. 6. Time stability of the PEC reactor in terms of linear sweep voltammetry variation over time. Inset: time variation of the photocurrent at 4 V.

Declaration of Competing Interest

The authors declare that they have no known competing financial interests or personal relationships that could have appeared to influence the work reported in this paper.

Data Availability

Data will be made available on request.

Acknowledgments

This work received financial support from the University of Milano (SEED 2019 project No. 1148) and from the PRIMA 2019 FishPhotoCat Project. The authors thank Nanomaterials S.r.l. (Milano) for the PEC prototype.

Appendix A. Supporting information

Supplementary data associated with this article can be found in the online version at doi:10.1016/j.cattod.2023.01.003.

References

[1] N. Adams, D. Bealing, Organic pollution: biochemical oxygen demand and ammonia, Handb. Ecotoxicol. 2–2 (2009) 728–749, https://doi.org/10.1002/9781444313512.CH33.
[2] M. Constable, M. Charlton, F. Jensen, K. McDonald, G. Craig, K.W. Taylor, An ecological risk assessment of ammonia in the aquatic environment, Hum. Ecol. Risk Assess. 9 (2003) 527–548, https://doi.org/10.1080/713609921.
[3] J.A. Camargo, Á. Alonso, Ecological and toxicological effects of inorganic nitrogen pollution in aquatic ecosystems: a global assessment, Environ. Int. 32 (2006) 831–849, https://doi.org/10.1016/J.ENVINT.2006.05.002.
[4] M.P. Lesser, Oxidative stress in marine environments: biochemistry and physiological ecology, Annu. Rev. Physiol. 68 (2006) 253–278, https://doi.org/10.1146/ANNUREV.PHYSIOL.68.040104.110001.
[5] V.M. Kensa, Bioremediation–an overview, J. Ind. Pollut. Control. 27 (2011) 161–168.
[6] P. Chávez-Crooker, J. Obreque-Contreras, Bioremediation of aquaculture wastes, Curr. Opin. Biotechnol. 21 (2010) 313–317, https://doi.org/10.1016/J.COPBIO.2010.04.001.
[7] R. Andreozzi, V. Caprio, A. Insola, R. Marotta, Advanced oxidation processes (AOP) for water purification and recovery, Catal. Today 53 (1999) 51–59, https://doi.org/10.1016/S0920-5861(99)00102-9.
[8] R. Crab, Y. Avnimelech, T. Defoirdt, P. Bossier, W. Verstraete, Nitrogen removal techniques in aquaculture for a sustainable production, Aquaculture 270 (2007) 1–14, https://doi.org/10.1016/J.AQUACULTURE.2007.05.006.
[9] K. Vikrant, K.H. Kim, F. Dong, D.A. Giannakoudakis, Photocatalytic platforms for removal of ammonia from gaseous and aqueous matrixes: status and challenges,

ACS Catal. 10 (2020) 8683–8716, https://doi.org/10.1021/ACSCATAL.0C02163/ASSET/IMAGES/LARGE/CS0C02163_0014.JPEG.
[10] X. Gong, H. Wang, C. Yang, Q. Li, X. Chen, J. Hu, Photocatalytic degradation of high ammonia concentration wastewater by TiO_2, Future Cities Environ. 1 (2015) 12, https://doi.org/10.1186/S40984-015-0012-9.
[11] S. Horikoshi, N. Serpone, Can the photocatalyst TiO_2 be incorporated into a wastewater treatment method? Background and prospects, Catal. Today 340 (2020) 334–346, https://doi.org/10.1016/J.CATTOD.2018.10.020.
[12] X. Peng, M. Wang, F. Hu, F. Qiu, H. Dai, Z. Cao, Facile fabrication of hollow biochar carbon-doped TiO_2/CuO composites for the photocatalytic degradation of ammonia nitrogen from aqueous solution, J. Alloy. Compd. 770 (2019) 1055–1063, https://doi.org/10.1016/J.JALLCOM.2018.08.207.
[13] T. Du, G. Zhang, J. Zou, Coupling photocatalytic and electrocatalytic oxidation towards simultaneous removal of humic acid and ammonia–nitrogen in landscape water, Chemosphere 286 (2022), 131717, https://doi.org/10.1016/J.CHEMOSPHERE.2021.131717.
[14] Z. Mohammadi, S. Sharifnia, Y. Shavisi, Photocatalytic degradation of aqueous ammonia by using TiO_2ZnO/LECA hybrid photocatalyst, Mater. Chem. Phys. 184 (2016) 110–117, https://doi.org/10.1016/J.MATCHEMPHYS.2016.09.031.
[15] Y. Shavisi, S. Sharifnia, S.N. Hosseini, M.A. Khadivi, Application of TiO_2/perlite photocatalysis for degradation of ammonia in wastewater, J. Ind. Eng. Chem. 20 (2014) 278–283, https://doi.org/10.1016/J.JIEC.2013.03.037.
[16] B. Randazzo, G. Chemello, I. Tortarolo, G.L. Chiarello, M. Zalas, A. Santini, M. Liberatore, M. Liberatore, E. Selli, I. Olivotto, A Novel Photocatalytic Purification System for Fish Culture, vol. 14, 2017, pp. 411–21. ⟨Https://Home.Liebertpub.Com/Zeb⟩, ⟨https://doi.org/10.1089/ZEB.2017.1448⟩.
[17] E. Buoio, C. Cialini, A. Cafiso, L. Aidos, S.M. Mazzola, R. Rossi, S. Livolsi, A. di Giancamillo, V.M. Moretti, E. Selli, M. Bestetti, S. Franz, G.L. Chiarello, A. Costa, C. Bazzocchi, From photocatalysis to photo-electrocatalysis: an innovative water remediation system for sustainable fish farming, Sustainability 14 (2022), https://doi.org/10.3390/SU14159067.
[18] M. Altomare, G.L. Chiarello, A. Costa, M. Guarino, E. Selli, Photocatalytic abatement of ammonia in nitrogen-containing effluents, Chem. Eng. J. 191 (2012) 394–401, https://doi.org/10.1016/J.CEJ.2012.03.037.
[19] E. Zhang, X. Zhao, J. Hu, R. Wang, S. Fu, G. Qin, Antibacterial metals and alloys for potential biomedical implants, Bioact. Mater. 6 (2021) 2569–2612, https://doi.org/10.1016/J.BIOACTMAT.2021.01.030.
[20] M. Abu-Dalo, A. Jaradat, B.A. Albiss, N.A.F. Al-Rawashdeh, Green synthesis of TiO_2 NPs/pristine pomegranate peel extract nanocomposite and its antimicrobial activity for water disinfection, J. Environ. Chem. Eng. 7 (2019), https://doi.org/10.1016/J.JECE.2019.103370.
[21] M.C. Collivignarelli, A. Abbà, M. Carnevale Miino, G. Bertanza, S. Sorlini, S. Damiani, H. Arab, M. Bestetti, S. Franz, Photoelectrocatalysis on TiO_2 meshes: different applications in the integrated urban water management, Environ. Sci. Pollut. Res. 28 (2021) 59452–59461, https://doi.org/10.1007/S11356-021-12606-5.
[22] Y. Ji, J. Bai, J. Li, T. Luo, L. Qiao, Q. Zeng, B. Zhou, Highly selective transformation of ammonia nitrogen to N_2 based on a novel solar-driven photoelectrocatalytic-chlorine radical reactions system, Water Res. 125 (2017) 512–519, https://doi.org/10.1016/J.WATRES.2017.08.053.
[23] N. Kishimoto, Y. Katayama, M. Kato, H. Otsu, Technical feasibility of UV/electro-chlorine advanced oxidation process and pH response, Chem. Eng. J. 334 (2018) 2363–2372, https://doi.org/10.1016/J.CEJ.2017.11.108.
[24] S. Franz, H. Arab, G.L. Chiarello, M. Bestetti, E. Selli, Single-step preparation of large area TiO_2 photoelectrodes for water splitting, Adv. Energy Mater. 10 (2020) 2000652, https://doi.org/10.1002/AENM.202000652.
[25] S. Franz, D. Perego, O. Marchese, A. Lucotti, M. Bestetti, Photoactive TiO_2 coatings obtained by plasma electrolytic oxidation in refrigerated electrolytes, Appl. Surf. Sci. 385 (2016) 498–505, https://doi.org/10.1016/J.APSUSC.2016.05.032.
[26] G.L. Chiarello, M. Bernareggi, M. Pedroni, M. Magni, S.M. Pietralunga, A. Tagliaferri, E. Vassallo, E. Selli, Enhanced photopromoted electron transfer over a bilayer WO_3 n–n heterojunction prepared by RF diode sputtering, J. Mater. Chem. A Mater. 5 (2017) 12977–12989, https://doi.org/10.1039/C7TA03887A.
[27] M. Altomare, G.L. Chiarello, A. Costa, M. Guarino, E. Selli, Photocatalytic abatement of ammonia in nitrogen-containing effluents, Chem. Eng. J. 191 (2012) 394–401, https://doi.org/10.1016/J.CEJ.2012.03.037.
[28] Y. Zhang, Y. Ji, J. Li, J. Bai, S. Chen, L. Li, J. Wang, T. Zhou, P. Jiang, X. Guan, B. Zhou, Efficient ammonia removal and toxic chlorate control by using $BiVO_4$/WO_3 heterojunction photoanode in a self-driven PEC-chlorine system, J. Hazard. Mater. 402 (2021), https://doi.org/10.1016/J.JHAZMAT.2020.123725.
[29] S. Wang, Z. Ye, F. Taghipour, UV photoelectrochemical process for the synergistic degradation of total ammonia nitrogen (TAN), J. Clean. Prod. 289 (2021), https://doi.org/10.1016/J.JCLEPRO.2020.125645.
[30] M. Kwon, A. Royce, Y. Gong, K.P. Ishida, M.I. Stefan, UV/chlorine vs. UV/H_2O_2 for water reuse at Orange County Water District, CA: a pilot study, Environ. Sci. 6 (2020) 2416–2431, https://doi.org/10.1039/D0EW00316F.